Science and Technology for Energy Transition **78**, 8 (2023)

https://doi.org/10.2516/stet/2023005

Selected Papers from First European Conference on Gas Hydrates (ECGH), 2022
Bertrand Chazallon and Anh Minh Tang (Guest Editors)

Available online at:
stet-review.org

REGULAR ARTICLE OPEN ACCESS

CO_2 hydrate formation in NaCl systems and undersaturated aqueous solutions

Rod Burgass[1], Antonin Chapoy[1,2,*], Kjell M. Askvik[3], Bengt Olav Neeraas[3], and Xiaoyun Li[3]

[1] Hydrates, Flow Assurance & Phase Equilibria Research Group, Institute of GeoEnergy Engineering, Heriot-Watt University, Edinburgh EH14 4AS, UK
[2] Mines ParisTech, PSL University, CTP – Centre of Thermodynamics of Processes, 35 Rue Saint, Honoré 77305, Fontainebleau Cdex France
[3] Equinor ASA, Arkitekt Ebbells veg 10, 7053 Ranheim, Trondheim, Norway

Received: 26 September 2022 / Accepted: 2 March 2023

Abstract. A high-pressure experimental setup was used to obtain experimental data on the Hydrate Equilibrium (melting) Temperature (HET) of aqueous phases undersaturated with CO_2, at different CO_2 saturation levels and with different aqueous phase compositions (sodium chloride and sodium chloride/calcium chloride). This paper details the experimental equipment, methods, test fluids, and results. To study the phase equilibria of CO_2-brine systems and further validate the results, hydrate dissociation conditions of CO_2 in different concentrations of NaCl aqueous solutions were measured in the low-temperature region and over a wide range of pressure. Experimental results were compared against predictions of the simplified Cubic Plus Association Equation of State (sCPA-EoS) coupled with the van der Waals and Platteeuw solid solution theory.

Keywords: Carbon dioxide, Gas solubility, Hydrates.

1 Introduction

CO_2 injection in geological formations is a key aspect of the Carbon capture and Storage (CCS) strategy. The captured CO_2 will be injected into depleted oil and gas reservoirs and/or saline aquifers. The injection and potential CO_2 expansion can be associated with a large Joule–Thomson effect and may in turn pose a risk of hydrate or ice formation in the formation due to the cooling effect [1]. In addition, CO_2 can be injected/stored through Carbonated Water Injection technology [2], where CO_2 from offshore power production is captured from flue gas and compressed/injected into the geological formation as dissolved gas in the injection water. Hydrate could be formed in the injection water with dissolved CO_2.

Although different thermodynamic models have been developed to predict the carbon dioxide hydrate stability in aqueous NaCl solutions, high-accuracy experimental data are always necessary to validate or improve these predictive tools. Experimental data for carbon dioxide hydrates in equilibrium with sodium chloride solutions have been measured and reported by various authors in different hydrate regions. Table 1 gives a list of these data, reporting the temperature range and source of the experimental data. Available experimental data in the literature for CO_2 in NaCl aqueous solutions have mostly been measured at low pressures below the saturation lines. As seen in the table, data for high salinity are also limited.

In this study, experimental investigations were conducted to measure the hydrate stability zone of CO_2 in NaCl solutions over a wide range of conditions, in particular, to fill the gaps above the liquid locus and at high salinity. Moreover, experimental data on the hydrate equilibrium temperature of aqueous phases undersaturated in CO_2 with different CO_2 saturations and different aqueous phase compositions were carried out in order to validate and complement the available literature data (Tab. 2).

The Cubic-Plus-Association (CPA-EoS) Equation of State combined with the solid solution theory of van der Waals and Platteeuw [27] as developed by Parrish and Prausnitz [28] was employed to model the fluid and hydrate phase equilibria as previously described by Chapoy *et al.* [29–32]. The predictions of the thermodynamic model were compared with the newly experimentally measured properties.

* Corresponding author: a.chapoy@hw.ac.uk

Table 1. Literature data for hydrate equilibria of CO_2 in presence of NaCl solutions (VL_wH: Vapour – Liquid (aqueous) – Hydrate / LL_wH: Liquid – Liquid (aqueous) – Hydrate).

References	T (K)	P (MPa)	NaCl wt%	Types of equilibrium
Saji *et al.* [3]	274.0–279.5	1.65–3.78	3, 6	VL_wH
Dholabhai *et al.* [4]	263.3–280.9	1.16–3.91	3, 5, 10, 15, 20	VL_wH
Englezos and Hall [5]	267.45–277.35	1.15–3.7	10, 15.2	VL_wH
Vaessen *et al.* [6]	258.15–262.15	1.19–2.15	25	VL_wH
Sun *et al.* [7]	276.15–278.15	1.93–2.86	4	VL_wH
Nakane *et al.* [8]	271.95–279.5	1.6–2.96	3.5, 7, 10	VL_wH
Tohidi *et al.* [9]	263.2–276.0	1.52–3.23	10, 20	VL_wH
Guembaroski *et al.* [10]	272.15–279.15	1.44–3.92	2, 5, 10, 15	VL_wH
Croeser *et al.* [11]	271.4–279.4	1.31–3.59	5	VL_wH
Mohammadi *et al.* [12]	271.8–280.2	1.37–3.73	5	VL_wH
Cordeiro *et al.* [13]	278.1–282.51	8.5–25	5, 10	LL_wH
Ruffine and Trusler [14]	274.84–280.68	3.6–60.1	4.3	$VL_wH + LL_wH$
Sabil *et al.* [15]	267.55–277.11	0.8–3.6	5, 10	VL_wH
Bozzo *et al.* [16]	271.67–283.15	1.04–4.5	2.5, 5, 7.5, 10	VL_wH

Table 2. Literature data of CO_2 solubility in water and brines at hydrate–liquid water (HL_w) equilibrium.

References	T (K)	P (MPa)	CO_2 (mole %)	NaCl wt%
Aya *et al.* [17]	276.15–282.75	30	1.96–3.14	–
Yang *et al.* [18]	279–281	5–6.1	2.32–2.69	–
Servio and Englezos [19]	274.05–282.95	2–6	1.56–2.81	–
Lee *et al.* [20]	273.15–280.15	5–20	0.7–2.6	–
Someya *et al.* [21]	275.8–282.3	7–10	1.6–3	–
Kim *et al.* [22]	278.9–280.4	10.1–20.1	2.31–2.71	0, 5.6
Zhang *et al.* [23]	274.1–281.1	1.9–23.6	1.63–2.42	0, SW*
Guo *et al.* [24]	275–283.15	20	1.67–2.72	–
Sun *et al.* [25]	273.95–282.85	2–5	1.63–2.76	0, 1, 3, 3.6
Geng *et al.* [26]	276.2–285.2	5–90	1.71–3.22	–

*SW: Seawater (~2.4 wt% NaCl, 0.4 wt% Na_2SO_4, 0.5 wt% $MgCl_2$, 0.11 wt% $CaCl_2$).

2 Experimental section

2.1 Materials

The CO_2 used was supplied by *Air Products* and has a stated purity of 99.995%. The NaCl and $CaCl_2$ were both supplied by *Sigma–Aldrich* and have a stated purity of 99.5%. Distilled water was used in all tests. Details of the used fluids are given in Table 3.

2.2 Experimental apparatus

The tests were conducted using a fixed-volume, temperature-controlled rocking cell as described below. The experimental set-up is comprised of an equilibrium cell (Fig. 1), cryostat, rocking/pivot mechanism, and temperature/pressure recording equipment controlled by a PC. The equilibrium cell is a 300 mL titanium cylindrical pressure vessel with a mixing ball, mounted on a horizontal pivot with an associated stand for pneumatically controlled rocking through 180°. The rocking of the cell, and the subsequent movement of the mixing ball within it, ensures adequate mixing of the cell fluids.

The rig has a working temperature range of 203–323 K, with a maximum operating pressure of 69 MPa. Circulating coolant from a cryostat within a jacket surrounding the cell controls the cell temperature. The cryostat can maintain the cell temperature stability to within better than 0.05 K. To achieve good temperature stability, the jacket is insulated with polystyrene board while connecting pipe work is covered with plastic foam.

The temperature is measured and monitored using a PRT (Platinum Resistance Thermometer) located within the cooling jacket of the cell. The cell temperature is measured with an uncertainty of 0.1 K. A strain gauge pressure transducer with an uncertainty of 0.03 MPa is used

Table 3. Composition of the chemical used in this work.

Chemical Name	CAS number	Formula	Purity (mol%)	Supplier	Purification method
Deionized water	7732-18-5	H_2O	100	*PURELABDV25*	No further purification
Carbon dioxide	124-38-9	CO_2	99.995	*Air Products*	No further purification
Sodium chloride	7440-23-5	NaCl	≥99.5%	*Sigma–Aldrich*	No further purification
Calcium chloride	7440-70-2	$CaCl_2$	≥99.5%	*Sigma–Aldrich*	No further purification

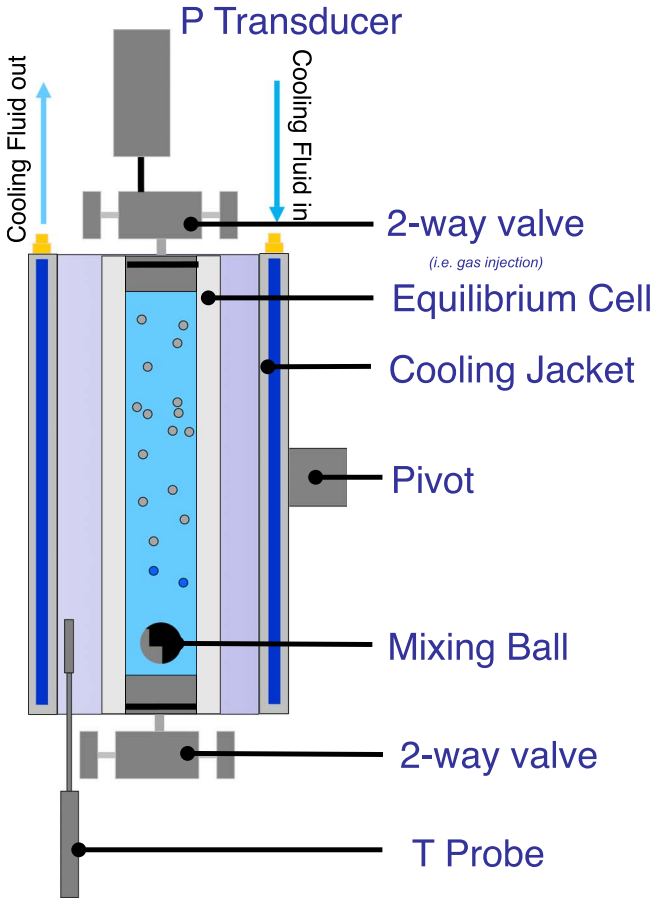

Fig. 1. Schematic of the setup used to measure the hydrate dissociation condition

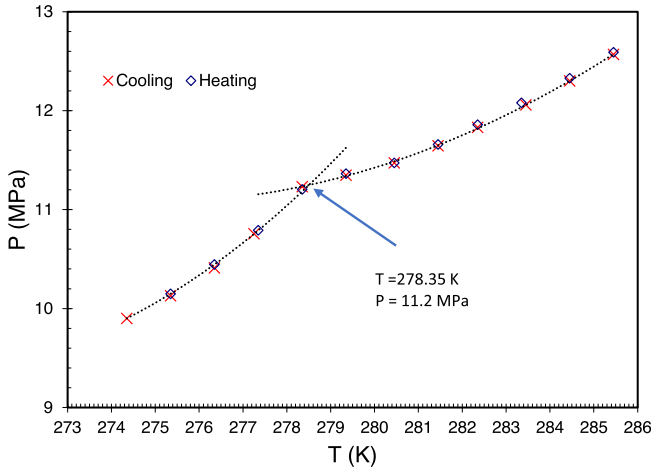

Fig. 2. Plot of equilibrium P/T data recorded during test $x_{CO2} = 2.11 \times 10^{-2}$ mole fraction in distilled water.

to monitor pressure. Temperature and Pressure are monitored and recorded by a PC through a RS 232 serial port. The cryostat can be monitored and controlled via an interface connected to a serial port on the computer. The temperature probe and pressure transducer are regularly calibrated using NAMAS certified temperature probe and a Budenberg dead weight tester, respectively.

2.3 Experimental methods

Hydrate dissociation point measurements for saturated systems were conducted using a reliable isochoric step-heating method as described in our previous papers [33, 34].

For undersaturated systems mixtures of CO_2 and aqueous phase, composed of either distilled water or water with salts were made in a separate 600 mL piston vessel. In the first instance, a measured amount of CO_2 was injected into the clean evacuated vessel. The amount of CO_2 was measured using a balance with a precision of 0.01 g. The aqueous phase was then pumped into the vessel using a Quizix high-pressure pump. The volume of injected liquid was determined according to the density of the aqueous phase and the desired CO_2 concentration. The weight of the aqueous phase injected into the vessel was checked using the balance. This method gave an uncertainty of ±0.05 weight % for the mixtures used in this study. The pressure of the mixture was increased by injecting nitrogen into the vessel on the opposite side of the piston to the test fluid. The pressure was increased at least 14 MPa above the expected bubble point of the mixture and was mixed for at least 30 min to ensure it was a single phase. The equilibrated mixture was then transferred to the rocking cell. During the transfer, the pressure of the mixture in the 600 mL cell and the test fluid pressure was maintained at a pressure at least 14 MPa above the expected bubble point to ensure it was always a single phase.

Once the test fluids had been loaded into the test cell the pressure and temperature were adjusted in order to make a HET measurement. The pressure was adjusted by injecting or withdrawing equilibrated fluid into the vessel. The cell was then rocked to achieve equilibrium before lowering the temperature stepwise below the expected HET temperature. The presence of hydrates was indicated by a change in the P *versus* T trend as shown in Figure 2.

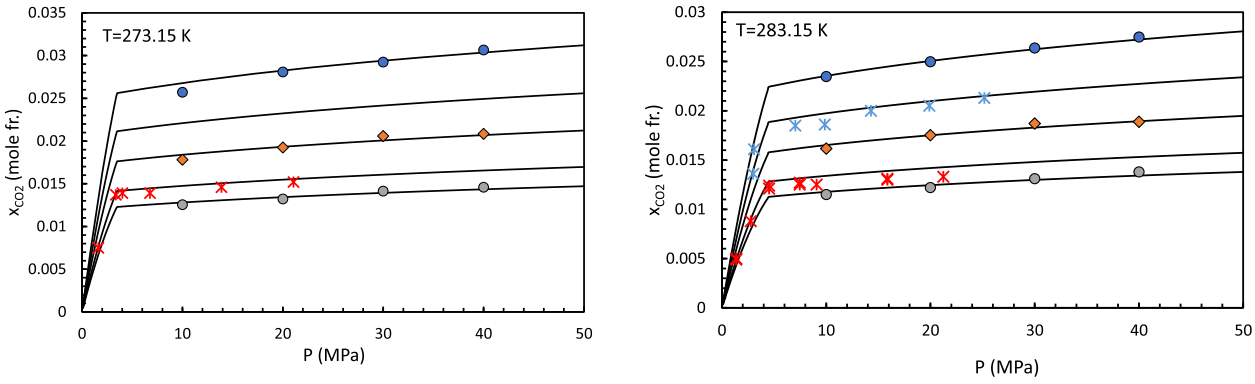

Fig. 3. Predicted and experimental CO_2 solubility in aqueous sodium chloride. Black lines: predictions using the CPA-EoS model. ●: 5.52 wt% NaCl [24]; ◆: 14.92 wt% NaCl [24]; ●: 22.61 wt% NaCl [24]; ✱: 10 wt% NaCl (Heriot–Watt unpublished data); ✱: 20 wt% NaCl (Heriot–Watt unpublished data).

Table 4. Experimental CO_2 hydrate dissociation conditions in the presence of sodium chloride solutions (AqFr: Aqueous Fraction).

wt% NaCl	AqFr	T_D/K	P_D/MPa	Type of equilibrium
5	0.990	270.7	1.149	VL_wH
	0.984	274.2	1.736	VL_wH
	0.979	275.9	2.180	VL_wH
	0.974	277.3	2.599	VL_wH
	0.966	278.9	3.243	VL_wH
	0.942	280.6	4.226	VL_wH
10	0.990	266.9	0.994	VL_wH
	0.987	269.7	1.390	VL_wH
	0.980	272.3	1.882	VL_wH
	0.976	274.4	2.479	VL_wH
15	0.992	266.25	1.200	VL_wH
	0.774	274.15	7.570	LL_wH
	0.764	275.75	19.477	LL_wH
20	0.996	259.95	0.896	VL_wH
	0.993	264.05	1.503	VL_wH
	0.988	267.15	2.248	VL_wH
	0.828	269.45	6.026	LL_wH
	0.826	270.05	8.832	LL_wH
	0.826	270.25	8.846	LL_wH
	0.821	270.55	16.830	LL_wH
23	0.987	254.75	0.703	VL_wH
	0.974	260.75	1.434	VL_wH
	0.941	265.95	2.848	VL_wH
	0.535	269.75	28.924	LL_wH
25	0.955	261.75	1.875	VL_wH
	0.693	263.85	4.592	LL_wH
	0.635	264.05	7.219	LL_wH
	0.811	264.95	12.038	LL_wH
	0.799	265.75	29.316	LL_wH

Expanded uncertainties ($k = 2$): $u(T_D) = 0.4$ K, $u(P_D) = 0.13$ MPa, u(wt% NaCl) = 0.01. See Appendix.

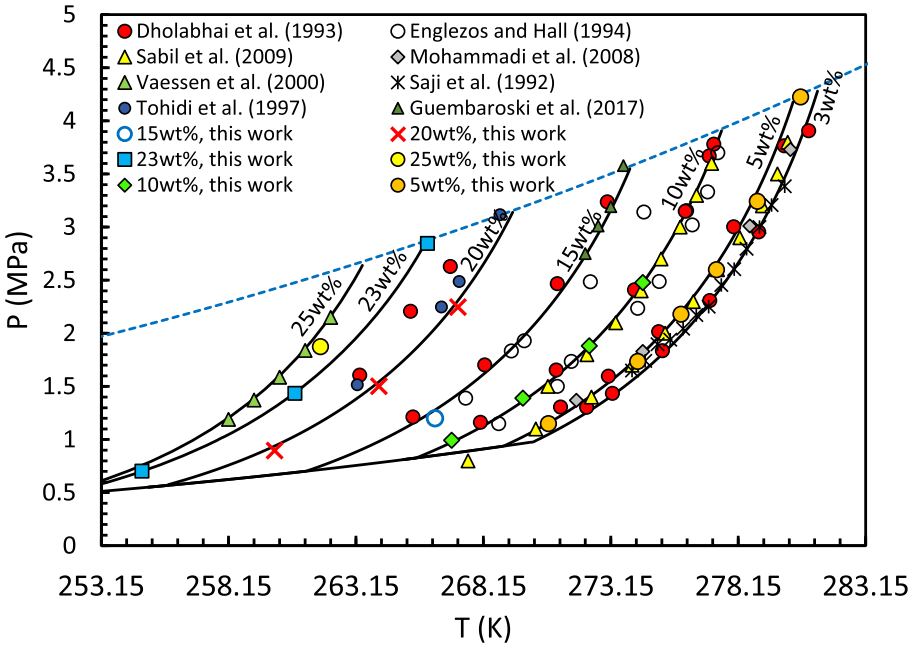

Fig. 4. Predicted and experimental hydrate stability of the CO_2 system in presence of aqueous sodium chloride solution in the VL_wH region; Black lines: hydrate stability zone predicted using the CPA-EoS model using an aqueous mole fraction of 0.8; dotted blue lines: vapour–liquid locus of CO_2 (no water) using the CPA-EoS model.

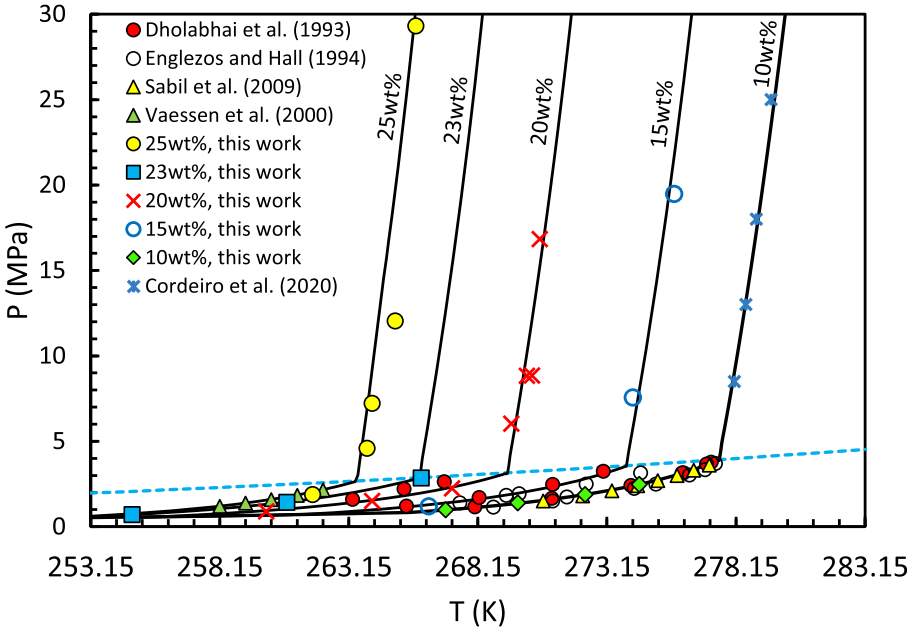

Fig. 5. Predicted and experimental hydrate stability of the CO_2 system in presence of aqueous sodium chloride solution in VLH and LLH regions; black lines: hydrate stability zone predicted using the CPA-EoS model using an aqueous mole fraction of 0.8; dotted blue lines: vapour–liquid locus of CO_2 (no water) using the CPA-EoS model.

Table 5. Hydrate equilibrium temperatures at HL_w as function of CO_2 concentration (x_{CO2}) in distilled water and saline systems (CO_2 concentration is on free-salt basis and mole fraction).

Aqueous composition	T (K)	P (MPa)	Wt% CO_2	$x_{CO2} \times 10^2$
Distilled water	274.05	9.51	4	1.677
	274.25	17.75	4	1.677
	275.75	10.23	4.4	1.849
	275.95	21.11	4.4	1.849
	278.15	8.34	5	2.109
	278.35	11.2	5	2.109
	278.55	19.17	5	2.109
	279.25	10.24	5.5	2.327
	279.45	20.34	5.5	2.327
	280.05	9.75	6	2.546
	280.35	15.45	6	2.546
3 wt% NaCl	271.45	10.47	3	1.250
	271.65	21.79	3	1.250
	277.15	11.28	4	1.677
	277.25	18.2	4	1.677
	277.95	10.96	5	2.109
	278.15	19.31	5	2.109
	279.35	9.35	6	2.546
	279.65	17.15	6	2.546
6 wt% NaCl	277.15	8.41	5	2.109
	277.55	15.61	5	2.109
3 wt% NaCl + 0.6 wt% $CaCl_2$	275.65	9.56	4	1.677
	275.85	20.41	4	1.677
	278.85	10.36	5	2.109
	278.95	13.51	5	2.109
	280.55	10.58	6	2.546
	280.75	14.38	6	2.546

Expanded uncertainties ($k = 2$): $u(T) = 0.7$ K, $u(P) = 0.13$ MPa, $u(x_{CO2} \times 10^2) = 0.04$. See Appendix.

The temperature was then increased stepwise allowing sufficient time for equilibrium to be achieved at each step. The equilibrium P/T data were then plotted to determine the point at which hydrates are no longer present as indicated by a change in the P *versus* T plot. An example is shown in Figure 2 below.

3 Thermodynamic modeling

A general phase equilibrium model based on the uniformity of component fugacities in all phases is used to predict phase equilibria, water activity, and the hydrate forming conditions. A description of the thermodynamic model and parameters can be found elsewhere [29–32]. The model has been validated against carbon dioxide hydrate dissociation data [35] and gas solubility in brines at temperatures above the carbon dioxide critical temperature [36]. The model can also predict the gas solubility at low temperatures ($T < 283.15$ K) with an excellent agreement as seen in Figure 3.

4 Results and discussions

The experimental hydrate dissociations for CO_2 in equilibrium with 5, 10, 15, 20, 23, and 25 wt% sodium chloride solutions are reported in Table 4 and plotted in Figures 4 and 5. In the vapor region (Fig. 4) the model is in excellent agreement with our new experimental data and most of the available literature data, with typical agreement better than 0.5 K. For the 25 wt% solutions, the problem is more complex as when the system is cooled down the system forms $NaCl{\cdot}2H_2O$ before clathrate hydrates and the concentration in salt will therefore decrease in the remaining aqueous phase until it reaches the eutectic concentration 23.2 wt%, nevertheless taking into account the salting-out effect the model can still predict the dissociation conditions. In the liquid region (Fig. 5), errors between models and experimental results are slightly higher, however not greater than 1 K.

Table 5 gives a summary of the measurements made in this work for undersaturated systems. As can be seen, in all cases increasing the pressure leads to an increase in the

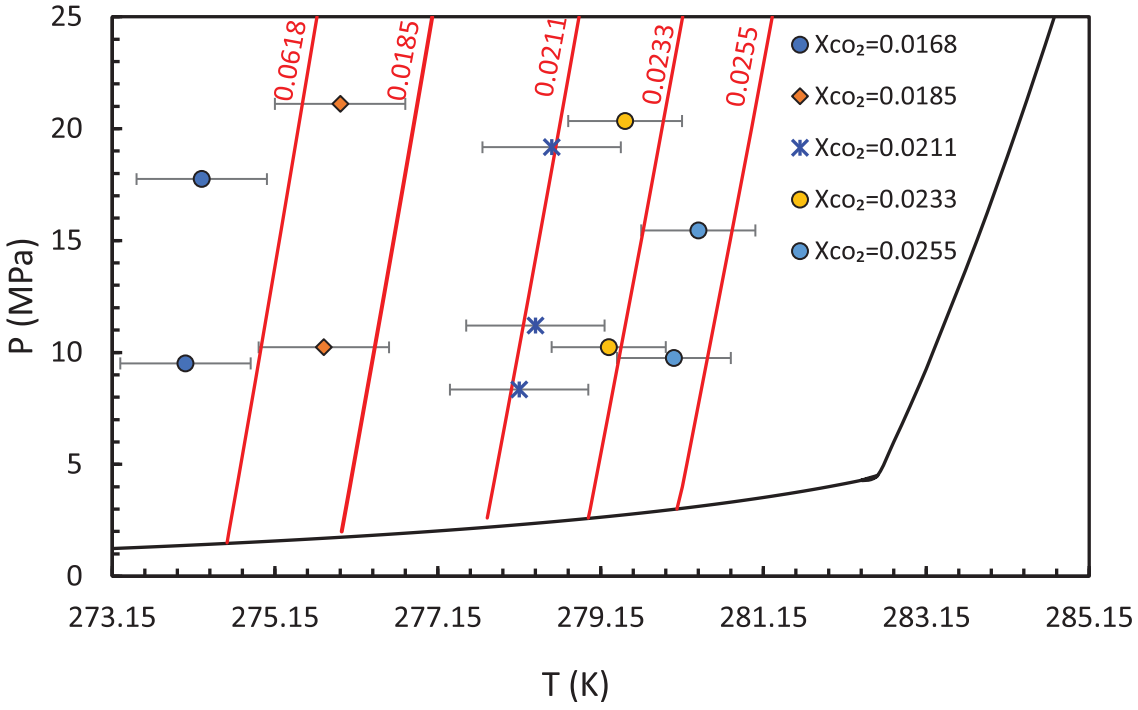

Fig. 6. Experimental and predicted hydrate equilibrium temperature at CO_2 isopleth (x_{CO2} is in mol fraction) in distilled water (red lines: HL_w predictions; black lines: VHL_w/LHL_w predictions).

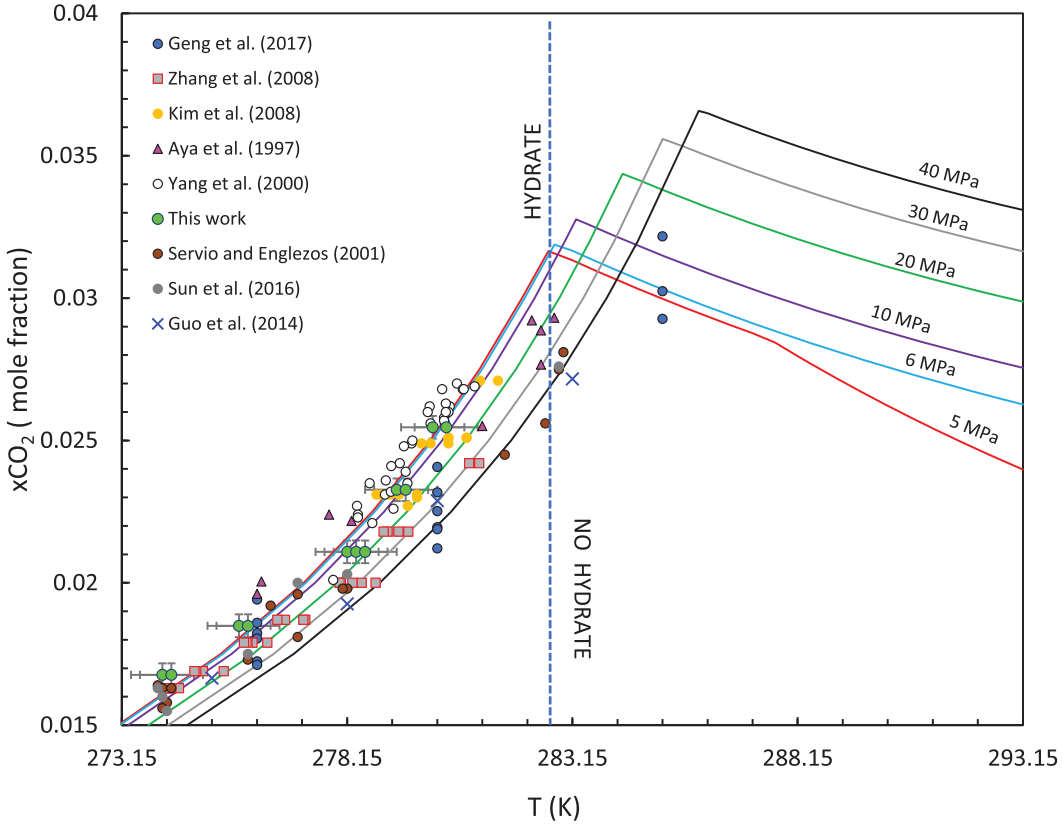

Fig. 7. Comparison of experimental and predicted solubility of CO_2 in water at H–L_w and V–L_w equilibria.

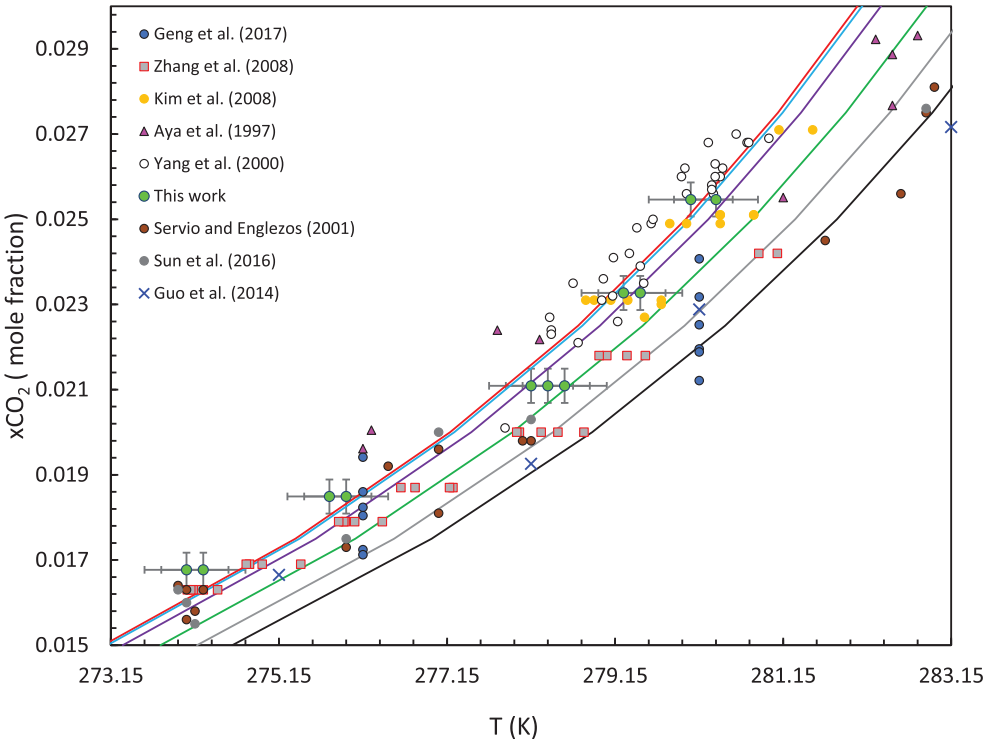

Fig. 8. Comparison of experimental and predicted solubility of CO_2 in water at H–L_w equilibria at 5, 6, 10, 20, 30, and 40 MPa (lines from left to right).

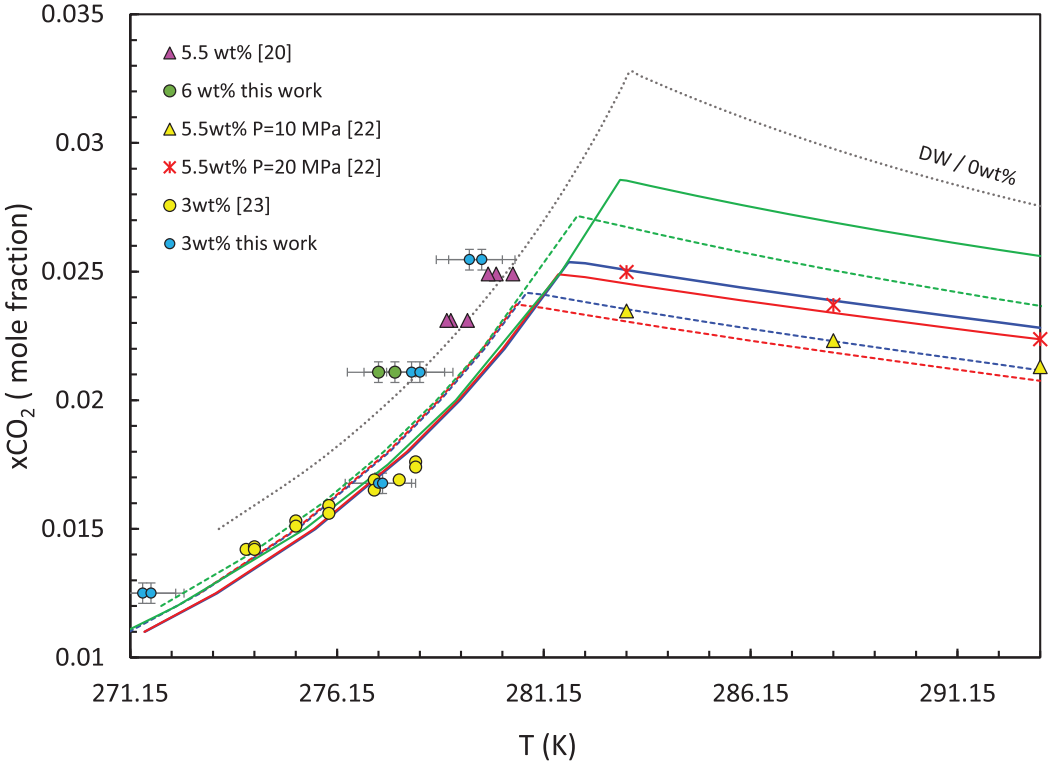

Fig. 9. Comparison of experimental and predicted solubility of CO_2 in NaCl aqueous solutions at H–L_w equilibria (grey dashed lines predictions for distilled water at 10 MPa; green lines: predictions for 3 wt% NaCl at 10 (dashed) and 20 MPa; blue lines: predictions for 5.52 wt% NaCl at 10 (dashed), and 20 MPa; red lines: predictions for 6 wt% NaCl at 10 (dashed) and 20 MPa).

HET for the saturated system. All of the data for distilled water are summarized in Figures 6–8 showing the effect of CO_2 saturation on HET for the tests with distilled water. The deviations between the measured HET and model predictions for distilled water are on average lower than 0.5 K and a maximum of 1 K for the lowest CO_2 concentration.

For salt solutions, the results are plotted in Figure 9 where larger deviations between experimental data and model predictions are observed. For some CO_2 concentrations, the measured HET increases with increasing salinity, while the model predicts the opposite behavior. There is a need for further experimental measurements and model development for aqueous systems undersaturated with CO_2.

5 Conclusion

In this work, new experimental data have been reported for hydrates formed from carbon dioxide in the presence of aqueous solutions of sodium chloride over a wide range of temperatures, pressure, and concentration. The predictions of the developed model are compared against independent experimental data and the data generated in this work over a wide range of temperature, pressure, and NaCl concentration. A good agreement between predictions and experimental data is observed, demonstrating the reliability of the developed model. The hydrate stability pressure–temperature zone of dissolved CO_2 in the presence of salt show that a decrease in the system pressure and/or an increase in salt concentration favors hydrate formation, as both factors reduce equilibrium gas solubility in the aqueous phase. This behavior is unlike that of the system including a gas phase, where a higher gas pressure corresponds to an increased gas solubility which favors hydrate formation.

To further validate the model, Hydrate Equilibrium (melting) Temperature (HET) of aqueous phases undersaturated with CO_2, at different CO_2 saturation levels and with different aqueous phase compositions were measured. The model is in relatively good agreement with the experimental results for distilled water, but larger deviations are observed for saline systems highlighting the need for further work to improve the model.

Acknowledgments. Some of this work was part of a Joint Industrial Project (JIP) conducted jointly at the *Institute of GeoEnergy Engineering*, *Heriot-Watt University*, and the CTP laboratory of *MINES ParisTech* between 2018 and 2021. The JIP was supported by *Equinor*, *GALP Energia*, *Linde AG*, *Petrobras*, *Petronas*, and *TOTAL*, which is gratefully acknowledged. HET measurements for undersaturated measurements were financed by *Equinor*.

References

1 Maloney D.R., Briceno M. (2009) Experimental investigation of cooling effects resulting from injecting high pressure liquid or supercritical CO_2 into a low pressure gas reservoir1, *Petrophysics* **50**, 335–344.

2 Sohrabi M., Riazi M., Jamiolahmady M., Ireland S., Brown C. (2009) Enhanced oil recovery and CO_2 storage by carbonated water injection, in: Int. Pet. Technol. Conf., IPTC, December 7–9, Doha, 14070 p. https://doi.org/10.2523/IPTC-14070-ABSTRACT.

3 Saji A., Yoshida H., Sakai M., Tanii T., Kamata T., Kitamura H. (1992) Fixation of carbon dioxide by clathrate-hydrate, *Energy Convers. Manag.* **33**, 643–649. https://doi.org/10.1016/0196-8904(92)90067-7.

4 Dholabhai P.D., Kalogerakis N., Bishnoi P.R. (1993) Equilibrium conditions for carbon dioxide hydrate formation in aqueous electrolyte solutions, *J. Chem. Eng. Data.* **38**, 650–654. https://doi.org/10.1021/je00012a045.

5 Englezos P., Hall S. (1994) Phase equilibrium data on carbon dioxide hydrate in the presence of electrolytes, water soluble polymers and montmorillonite, *Can. J. Chem. Eng.* **72**, 887–893. https://doi.org/10.1002/cjce.5450720516.

6 Vaessen R.J.C., Ham F., Witkamp G.J. (2000) Eutectic freeze crystallization using CO_2 clathrates, *Ann. N. Y. Acad. Sci.* **912**, 483–495. https://doi.org/10.1111/j.1749-6632.2000.tb06803.x.

7 Sun D., Ripmeester J., Englezos P. (2016) Phase equilibria for the $CO_2/CH_4/N_2/H_2O$ system in the hydrate region under conditions relevant to storage of CO_2 in depleted natural gas reservoirs, *J. Chem. Eng. Data.* **61**, 4061–4067. https://doi.org/10.1021/acs.jced.6b00547.

8 Nakane R., Gima E., Ohmura R., Senaha I., Yasuda K. (2019) Phase equilibrium condition measurements in carbon dioxide hydrate forming system coexisting with sodium chloride aqueous solutions, *J. Chem. Thermodyn.* **130**, 192–197. https://doi.org/10.1016/j.jct.2018.10.008.

9 Tohidi B., Danesh A., Todd A.C., Burgass R.W. (1997) Hydrate-free zone for synthetic and real reservoir fluids in the presence of saline water, *Chem. Eng. Sci.* **52**, 3257–3263. https://doi.org/10.1016/S0009-2509(97)00183-8.

10 Guembaroski A.Z., Marcelino Neto M.A., Bertoldi D., Morales R.E.M., Sum A.K. (2017) Phase behavior of carbon dioxide hydrates: A comparison of inhibition between sodium chloride and ethanol, *J. Chem. Eng. Data.* **62**, 3445–3451. https://doi.org/10.1021/acs.jced.7b00463.

11 Croeser N., Babaee S., Naidoo P., Ramjugernath D. (2019) Investigation into the use of gas hydrate technology for the treatment of vinasse, *Fluid Phase Equilib.* **492**, 67–77. https://doi.org/10.1016/j.fluid.2019.02.020.

12 Mohammadi A.H., Afzal W., Richon D. (2008) Gas hydrates of methane, ethane, propane, and carbon dioxide in the presence of single NaCl, KCl, and $CaCl_2$ aqueous solutions: Experimental measurements and predictions of dissociation conditions, *J. Chem. Thermodyn.* **40**, 1693–1697. https://doi.org/10.1016/j.jct.2008.06.015.

13 Cordeiro J.C., Marcelino Neto M.A., Morales R.E.M., Sum A.K. (2020) Phase equilibrium of carbon dioxide hydrates inhibited with MEG and NaCl above the upper quadruple point, *J. Chem. Eng. Data.* **65**, 280–286. https://doi.org/10.1021/acs.jced.9b01001.

14 Ruffine L., Trusler J.P.M. (2010) Phase behaviour of mixed-gas hydrate systems containing carbon dioxide, *J. Chem. Thermodyn.* **42**, 605–611. https://doi.org/10.1016/j.jct.2009.11.019.

15 Sabil K.M., Witkamp G.J., Peters C.J. (2009) Phase equilibria of mixed carbon dioxide and tetrahydrofuran hydrates in sodium chloride aqueous solutions, *Fluid Phase Equilib.* **284**, 38–43. https://doi.org/10.1016/j.fluid.2009.06.006.

16 Bozzo A.T., Hsiao-Sheng C., Kass J.R., Barduhn A.J. (1975) The properties of the hydrates of chlorine and carbon dioxide, *Desalination* **16**, 303–320. https://doi.org/10.1016/S0011-9164(00)88004-2.
17 Aya I., Yamane K., Nariai H. (1997) Solubility of CO_2 and density of CO_2 hydrate at 30 MPa, *Energy* **22**, 263–271. https://doi.org/10.1016/S0360-5442(96)00093-X.
18 Yang S.O., Yang I.M., Kim Y.S., Lee C.S. (2000) Measurement and prediction of phase equilibria for water + CO_2 in hydrate forming conditions, *Fluid Phase Equilib.* **175**, 75–89. https://doi.org/10.1016/S0378-3812(00)00467-2.
19 Servio P., Englezos P. (2001) Effect of temperature and pressure on the solubility of carbon dioxide in water in the presence of gas hydrate, *Fluid Phase Equilib.* **190**, 127–134. https://doi.org/10.1016/S0378-3812(01)00598-2.
20 Lee K.M., Lee H., Lee J., Kang J.M. (2002) CO_2 hydrate behavior in the deep ocean sediments; phase equilibrium, formation kinetics, and solubility, *Geophys. Res. Lett.* **29**, 30-1–30–4. https://doi.org/10.1029/2002GL015069.
21 Someya S., Bando S., Chen B., Song Y., Nishio M. (2005) Measurement of CO_2 solubility in pure water and the pressure effect on it in the presence of clathrate hydrate, *Int. J. Heat Mass Transf.* **48**, 2503–2507. https://doi.org/10.1016/j.ijheatmasstransfer.2004.12.043.
22 Kim Y.S., Lim B.D., Lee J.E., Lee C.S. (2008) Solubilities of carbon dioxide, methane, and ethane in sodium chloride solution containing gas hydrate, *J. Chem. Eng. Data.* **53**, 1351–1354. https://doi.org/10.1021/je800074z.
23 Zhang Y., Holder G.D., Warzinski R.P. (2008) Phase equilibrium in two-phase, water-rich-liquid, hydrate systems: Experiment and theory, *Ind. Eng. Chem. Res.* **47**, 459–469. https://doi.org/10.1021/ie070846c.
24 Guo H., Chen Y., Hu Q., Lu W., Ou W., Geng L. (2014) Quantitative Raman spectroscopic investigation of geo-fluids high-pressure phase equilibria: Part I. Accurate calibration and determination of CO_2 solubility in water from 273.15 to 573.15 K and from 10 to 120 MPa, *Fluid Phase Equilib.* **382**, 70–79. https://doi.org/10.1016/j.fluid.2014.08.032.
25 Sun Q., Tian H., Li Z., Guo X., Liu A., Yang L. (2016) Solubility of CO_2 in water and NaCl solution in equilibrium with hydrate. Part I: Experimental measurement, *Fluid Phase Equilib.* **409**, 131–135. https://doi.org/10.1016/j.fluid.2015.09.033.
26 Geng L., Qu K., Lu W., Jiang L., Chou I.M. (2017) In situ Raman spectroscopic study of the pressure effect on the concentration of CO_2 in water at hydrate-liquid water equilibrium up to 900 bar, *Fluid Phase Equilib.* **438**, 37–43. https://doi.org/10.1016/j.fluid.2017.02.005.
27 van der Waals J.H., Platteeuw J.C. (2007) Clathrate solutions, in: *Adv. Chem. Phys.*, Vol. **2**, pp. 1–57. https://doi.org/10.1002/9780470143483.ch1.
28 Parrish W.R., Prausnitz J.M. (1972) Dissociation pressures of gas hydrates formed by gas mixtures, *Ind. Eng. Chem. Process Des. Dev.* **11**, 26–35. https://doi.org/10.1021/i260041a006.
29 Chapoy A., Haghighi H., Burgass R., Tohidi B. (2012) On the phase behaviour of the (carbon dioxide + water) systems at low temperatures: Experimental and modelling, *J. Chem. Thermodyn.* **47**, 6–12. https://doi.org/10.1016/j.jct.2011.10.026.
30 Burgass R., Chapoy A., Duchet-Suchaux P., Tohidi B. (2014) Experimental water content measurements of carbon dioxide in equilibrium with hydrates at (223.15 to 263.15) K and (1.0 to 10.0) MPa, *J. Chem. Thermodyn.* **69**, 1–5. https://doi.org/10.1016/j.jct.2013.09.033.
31 Chapoy A., Nazeri M., Kapateh M., Burgass R., Coquelet C., Tohidi B. (2013) Effect of impurities on thermophysical properties and phase behaviour of a CO_2-rich system in CCS, *Int. J. Greenh. Gas Control.* **19**, 92–100. https://doi.org/10.1016/j.ijggc.2013.08.019.
32 Haghighi H., Chapoy A., Tohidi B. (2008) Freezing point depression of electrolyte solutions: Experimental measurements and modeling using the cubic-plus-association equation of state, *Ind. Eng. Chem. Res.* **47**, 3983–3989. https://doi.org/10.1021/ie800017e.
33 Haghighi H., Chapoy A., Tohidi B. (2009) Methane and water phase equilibria in the presence of single and mixed electrolyte solutions using the cubic-plus-association equation of State, *Oil Gas Sci. Technol.* **64**, 141–154. https://doi.org/10.2516/ogst:2008043.
34 Haghighi H., Chapoy A., Burgess R., Tohidi B. (2009) Experimental and thermodynamic modelling of systems containing water and ethylene glycol: Application to flow assurance and gas processing, *Fluid Phase Equilib.* **276**, 24–30. https://doi.org/10.1016/j.fluid.2008.10.006.
35 Chapoy A., Burgass R., Tohidi B., Alsiyabi I. (2015) Hydrate and phase behavior modeling in CO_2-rich pipelines, *J. Chem. Eng. Data.* **60**, 447–453. https://doi.org/10.1021/je500834t.
36 Ahmadi P., Chapoy A. (2018) Fluid phase equilibria CO_2 solubility in formation water under sequestration conditions, *Fluid Phase Equilib.* **463**, 80–90. https://doi.org/10.1016/j.fluid.2018.02.002.
37 JCGM (2008) Evaluation of measurement data – Guide to the expression of uncertainty in measurement, *Int. Organ. Stand. Geneva ISBN* **50**, 134.
38 Stringari P., Valtz A., Chapoy A. (2014) Study of factors influencing equilibrium and uncertainty in isochoric hydrate dissociation measurements, in: 8th Int. Conf. Gas Hydrates (ICGH8-2014), 28 July–1 August, Beijing, China, Vol. **28**.

Appendix

Temperature uncertainty

In this setup uncertainty of temperature measurement was calculated according to:

$$U_c(T) = \sqrt{u_{\text{thermometer}}{}^2 + u_{\text{calibration}}{}^2 + u_{\text{repeatability}}{}^2}. \quad \text{(A.1)}$$

The system, repeatability, and calibration uncertainties were found to be 0.1, 0.05, and 0.05 K, respectively. As a result, $U_c(T)$ was found to be 0.12 K for all points.

Pressure uncertainty:

Similar to the temperature uncertainty, the uncertainty of pressure measurements was calculated according to the following equations:

$$U_c(P) = \sqrt{u_{\text{system}}{}^2 + u_{\text{calibration}}{}^2 + u_{\text{repeatability}}{}^2}. \quad \text{(A.2)}$$

$U_c(P)$ was found to be 0.043 MPa with three digits accuracy for all the measurements.

HET for undersaturated systems

In this study, uncertainties of the measured hydrate equilibrium temperature were estimated based on the "Evaluation of Measurement Data – Guide to the Expression of Uncertainty in Measurement (GUM)" [37]. For HET measurements, considering the impact of uncertainties associated with calibration parameters, measured temperature, pressure, and sample preparation, the combined standard uncertainty of the measured density is calculated by:

$$u(T_{\mathrm{HET}})^2 = u(T)^2_{\mathrm{calibration}} + u(T)^2_{\mathrm{measurements}}. \tag{A.3}$$

For the calibration uncertainties, the temperature probe was calibrated using a NAMAS-certified temperature probe. For the uncertainties of HET measurements, equation (A.4) was used to determine the standard uncertainties:

$$u^2(T_{\mathrm{HET}})_{\mathrm{measurements}} = \left(\frac{\partial T_{HET}}{\partial p}\right)^2 u^2(p) + \left(\frac{\partial T_{\mathrm{HET}}}{\partial T}\right)^2 u^2(T) + \left(\frac{\partial T}{\partial x}\right)^2 u^2(x_{\mathrm{CO2}}). \tag{A.4}$$

$\left(\frac{\partial T}{\partial x}\right)$ was calculated using the thermodynamic model. Considering the systematic uncertainties of measurement devices, the calibration procedures, and the reproducibility of the results, the standard uncertainties of the measured HET were found to be 0.74 K.

HET for saturated systems

For the uncertainties of HET measurements in presence of NaCl, the procedure described by Stringari *et al.* [38] was used, and the standard uncertainties of the measured HET were found to be 0.4 K.